A Novel Integrated Multi-Layer Cooling (IMLC) Structure for High Power Density Applications

Andrew Yurek, Wenbo Liu, Yang Chen, Bo Sheng, Xiang Zhou and Yan-Fei Liu, *Fellow, IEEE*
Department of Electrical and Computer Engineering
Queen's University, Kingston, Canada
13aty@queensu.ca, yanfei.liu@queensu.ca

***Abstract* — This paper proposes a new Integrated Multi-Layer Cooling (IMLC) thermomechanical structure for high power density applications. The IMLC structure includes three design objectives to maximize thermal performance while optimizing power density. First, multiple PCBs are stacked vertically to increase PCB surface area. Second, cold plate liquid cooling is integrated onto the bottom most PCB to increase heat transfer. Third, components are distributed based on heat generation to efficiently cool lossy components. PCB thermal resistances are estimated based on three dimensional orthogonal thermal conductivities. FEA based thermal simulation is conducted with single PCB design and two-layer IMLC design. A 1.3kW power converter prototype is constructed with a single-layer PCB design using integrated liquid cooling. In testing, efficiency is improved by 0.6% and high loss component temperature rise is decreased by 50% compared to an air-cooled design. A two-layer IMLC design achieves the same thermal performance while improving power density by 31%.**

Keywords – thermomechanical, power density, integrated liquid cooling, efficiency

I. INTRODUCTION

High power density power converters are becoming increasingly popular due to the high demand for compact electrified devices and vehicles [1][2]. Consequently, research has focused on improving power converters to achieve high power density and small size. To achieve high power density and small size, integration methods are used to combine passive and active devices [3][4]. Such compact devices make use of wide band gap switching devices (WBG) and high frequency magnetics to achieve higher switching frequency and therefore reduce size of bulky magnetic components [5][6][7].The industry is continually advancing towards higher power density devices as fabrication processes and new technologies emerge.

The primary challenge when increasing power density is achieving enough heat transfer for high loss components in an increasingly small package [8]. With decreasing size, component loss increases while component surface area decreases. Therefore, more heat is required to be transferred from a smaller available surface area. This challenge presents the opportunity for thermal management solutions to be designed that address these challenges and achieve high power density designs. Current designs exist that address these challenges by proposing cooling methods which improve on convection and radiation heat transfer. Materials are designed which increase thermal conductivity to allow for more efficient convective heat transfer to ambient [9][10].

Medium power level devices operate in the range of 1kW to 20kW for applications such as electric vehicles. These devices require high power density and compact size but demand strong thermal performance. Single solutions of conduction or convection are insufficient for such devices [11][12]. Liquid cooling solutions offer both convection and conduction which makes it an attractive solution. This solution reduces thermal resistance to ambient to achieve decreased temperature rise for higher power applications [13]. Research has focussed on improving liquid cooled designs by integrating the pump and heatsink [14] or improving copper plate heatsink technology [15][16]. Other research has focussed on reducing thermal expansion to increase liquid cooling lifespan [17] and testing different coolants to increase heat transfer [18].

Currently, solutions exist for integrated circuits and power modules, but few exist for power converters on PCB assemblies. Medium level power converters consist of the PCB, semiconductor devices, passive components and control circuitry with complicated 3D layouts. Cooling solutions have tried to improve fixed component cooling or PCB design exclusively instead of together. These methods also sacrifice power density to integrate liquid cooling. A new Integrated Multi-Layer Cooling (IMLC) structure is proposed to achieve optimal thermal performance and power density. A two-PCB structure is designed to optimize usable PCB area based on separating power semiconductor devices, magnetics, and low loss control circuit. This paper is organized into the following sections: Section II describes the IMLC structure principle; Section III presents finite element analysis (FEA) thermal results for liquid cooling performance; Section IV presents the protype with experimental results and two-PCB simulation and experimental verification; Section V concludes the paper.

II. PRINCIPLE OF IMLC STRUCTURE

A 1.3kW power converter is designed using the IMLC structure for high to low voltage conversion from 400 to 14V. The operating parameters are shown in Table 1. A two-transformer structure is used to manage high secondary side winding loss due to large load current [19]. GaN devices are used to increase switching frequency operation to reduce magnetic component size and increase overall power density and efficiency [20][21]. Liquid cooling is integrated to the bottom surface of the bottommost PCB using copper connections and thermal isolation paste. For a single-PCB design, the PCB must accommodate both passive components and active switches on the top layer surface, shown in Fig. 1. The switches and magnetics occupy more

978-1-7281-1842-0/19/$31.00 ©2019 IEEE

Table 1: Power converter physical parameters.

V_{in}	Output voltage V_{out}	Maximum current I_{out}	Switching frequency f_{sw}	Dissipated heat Pd	Dimensions one PCB (mm)	Dimensions two PCBs (mm)
400V	14V	95A	260~350kHz	55W	70*190*42	45*190*50

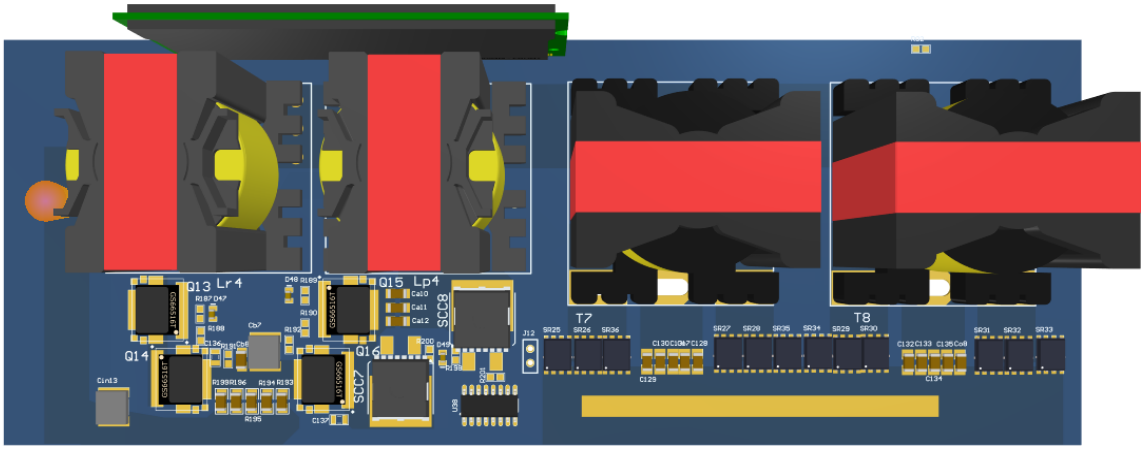

Fig. 1. Top view of conventional single PCB converter.

than half of the useable PCB surface area. In addition, a daughter card is required for control circuitry.

The objective of IMLC is to use package volume efficiently to reduce volume while maintaining thermal performance. This structure focusses on three design principles to achieve these objectives. First, IMLC uses two or more PCB's connected vertically through copper connections to utilize three-dimensional space and increase useable PCB surface area. Secondly, IMLC sorts and distributes components by heat generation, where high loss components are bonded to copper heat spreaders to dissipate the heat downwards. Finally, IMLC incorporates liquid cooling via cold plate heatsinking mounted to the bottom side of the bottommost PCB.

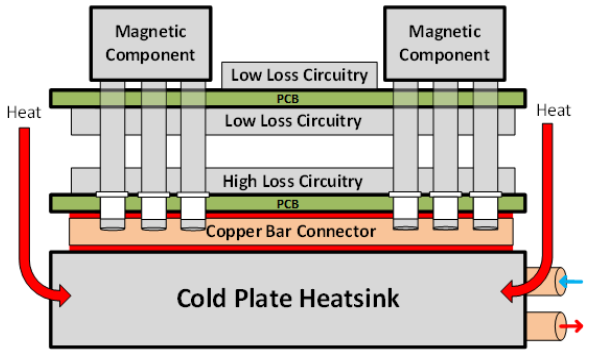

Fig. 2. Block diagram of IMLC structure.

Fig. 2 shows a diagram of the complete two-layer IMLC structure. IMLC allows for efficient placement of components according to loss. The top board is reserved for large magnetic components and low loss circuitry that provides control functions. Magnetic components are connected to the bottom board using copper connections electrically connected to both PCB layers. These connections also serve to anchor the bulky magnetic components to both PCB layers for support. On the bottom PCB layer, high loss surface mount components are exclusively placed on the top side to provide direct connection to the cold plate heatsink. Component height should be minimized to reduce the gap between PCBs and therefore minimize package volume. The entire bottom side of the bottom PCB is used to connect to the heatsink, except in areas with vertical copper connector protrusions.

IMLC incorporates active liquid cooling via a cold plate heatsink attached to the bottom side of the bottom PCB to transfer heat away from the converter. This connection is composed of the liquid cooled cold plate heatsink, thermal gap pads, copper bar connectors, and the bottom PCB. Copper bars allow a flush connection between the cold plate and PCB. Thermal gap pads are used to provide uniform contact, electric isolation and compensation of CTE mismatch. The two-layer structure allows for the converter width to be reduced while increasing the converter height by a relatively small amount. Therefore, package volume is significantly decreased. In the conventional single PCB structure, the total size is 0.56L with a power density of 2.33kW/L. For the IMLC converter the volume is 0.43L with 3.15kW/L power density. Converter size is reduced by 31% with same thermal performance and liquid cooling solution due to the component placement technique.

Fig. 3 shows the top view of the bottom layer PCB for the two PCB IMLC structure. The magnetics are located on the top side of top PCB and the switches are on the top side of bottom PCB. Fig. 4 shows the front cross section view of two- PCB stack. The control circuitry is located on the bottom side of the top PCB. A liquid cooling cold plate is assembled underneath the IMLC configured prototype with copper bar connection. The component size, surface area and contact area with the liquid cooled IMLC structure are unchanged from the single-PCB structure, therefore the same thermal performance can be achieved.

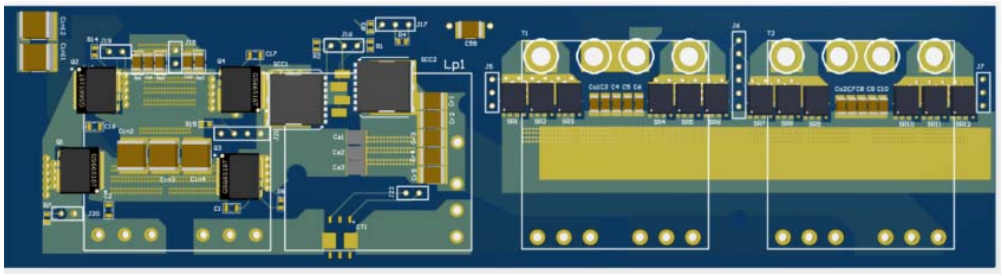

Fig. 3. Top view of IMLC bottommost PCB layer with high loss components.

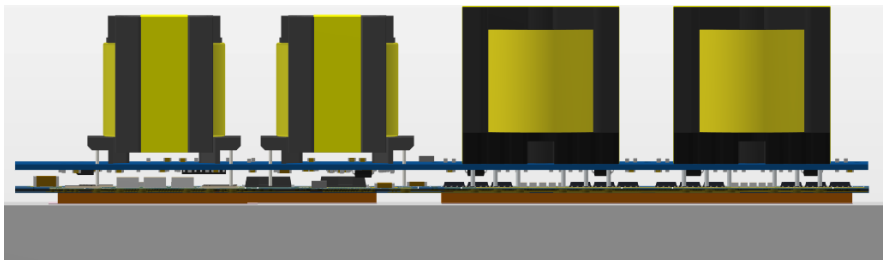

Fig. 4. Front view of IMLC structure.

III. Modeling and FEA Thermal Estimation Comparison

The thermal performance of the IMLC liquid cooling system is verified through FEA thermal simulation. Three simulations are performed to compare each PCB structure: conventional single PCB air cooled converter, single PCB liquid cooled converter, and IMLC liquid cooled converter. Three-dimensional models for each structure are created. The loss breakdown of the converter is also analyzed.

A. Orthogonally equivalized PCB thermal model

An equivalent thermal resistance method is used to simplify the PCB simulation model by approximating orthogonal thermal conductivity based on PCB thermal via distribution. Equation (1) below describes heat conduction inside a path.

$$q = \frac{T_1 - T_2}{d} \cdot \frac{g}{k \cdot A} \tag{1}$$

Where q (Watt) is the power of heat dissipation, T_1 and T_2 are the temperatures of the two terminals of the heat path, d is the length of heat path, g is the geometry factor which is represented as the effective contact area, and k (W/K.m) is the thermal conductivity of the heat carrier material. Equation (2) below express the conductive thermal resistance of a material.

$$R_{conduction} = g * \frac{d}{k * A} \tag{2}$$

Therefore, an equivalent thermal conductivity K_{eq} can be defined by the characterized thermal resistance $R_{conduction}$ for each structure using equation (3):

$$K_{eq} = {}^{d}/_{(A \cdot R_{conduction})} \tag{3}$$

The calculation of horizontal and vertical conductivity differs based on the heat transfer mechanism. Horizonal resistance occurs from the thermal resistance and FR4 in parallel because the heat transfers across multiple layers simultaneously. Vertical resistance appears as several resistances in series as the heat transfers through these layers continuously. Fig. 5 and Fig. 6 show the connection of horizonal and vertical thermal resistance respectively. The equivalent thermal resistance and conductivity are estimated based on this resistance network.

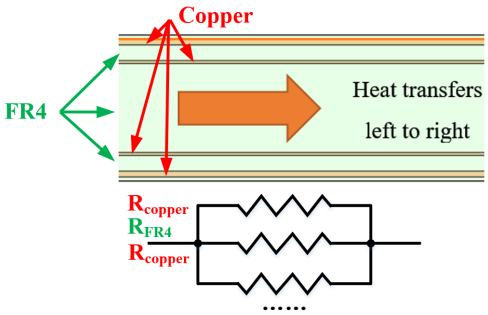

Fig. 5. Horizontal thermal resistance of PCB.

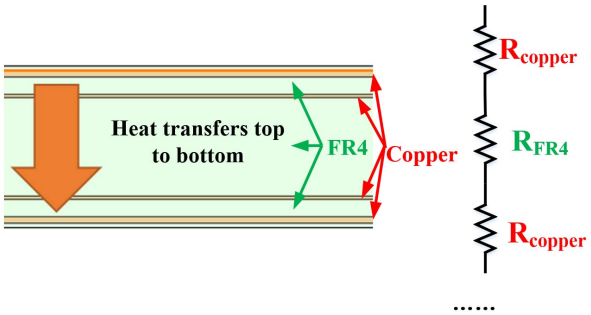

Fig. 6. Vertical thermal resistance of PCB.

The horizonal thermal resistance calculation is expressed in equation (4) as a parallel calculation with the total resistance of a length of *d*:

$$R_{PCB\_h} = R_{copper\_1} // R_{FR4\_1} // \ldots // R_{copper\_n} \tag{4}$$

Equation (5) expresses the horizontal equivalent thermal conductivity of PCB K_{eq_h}, derived from equation (4):

$$K_{eq\_h} = \frac{d}{A \; R_{PCB_h}} = \frac{t_{copper} K_{copper} + t_{FR4} K_{FR4}}{t_{PCB}} \tag{5}$$

Where t_{copper}, t_{FR4} and t_{PCB} are the thickness of copper layer, FR4, and PCB respectively. The vertical thermal resistance of a PCB with multiple copper layers of area *A* is calculated using equation (6):

$$R_{PCB\_v} = R_{copper\_1} + R_{FR4\_1} + \cdots + R_{copper\_n} \quad (6)$$

Thermal vias are placed underneath the critical high loss power semiconductor devices to improve thermal conductivity. This affects the vertical thermal resistance as heat transfers vertically across multiple vias at once. The resistance network is therefore the parallel of the PCB vertical resistance and via thermal resistance as shown in Fig. 7.

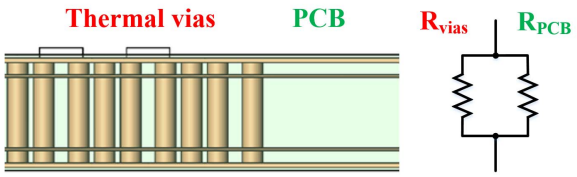

Fig. 7. Vertical thermal resistance of thermal vias and PCB.

Thus, the equivalent vertical thermal resistance of the PCB area with thermal vias is shown in equation (7):

$$R_{vertical} = R_{via} // R_{PCB\_v} \quad (7)$$

The equivalent vertical thermal conductivity of the PCB without and with thermal vias is expressed in equation (8) and (9) respectively:

$$K_{eq\_v1} = {}^{d}/_{(A \;\; R_{PCB\_v})} \quad (8)$$

$$K_{eq\_v2} = {}^{d}/_{(A \;\; R_{vertical})} \quad (9)$$

The PCB is segmented into pieces with and without thermal vias. Orthogonal equivalent thermal conductivity is defined by assigning K_{eq_h} for x and y direction and K_{eq_v} for z direction.

B. Loss break down and distribution

The loss of power converter is estimated for the 6 major components: primary GaN conduction and switching loss, resonant inductor (Lr) core and winding loss, parallel inductor (Lp) core and winding loss, transformer core and winding loss, secondary SR loss, and secondary copper loss.

The losses are estimated based on existing literature. The current and voltage values for each power components are simulated using PSIM software. Static and dynamic properties are extracted from component datasheets. The conduction loss and switching loss of GaN FETs are calculated based on I^2R and gate charging information. C_{oss} loss is estimated based on research in [22]. Magnetic core losses are calculated using Steinmetz's equation. Magnetic AC copper loss in high frequency is analyzed based on the study of proximity effect and skin effect in [23][24]. Transformer secondary side winding loss is estimated based on [25]. SR conduction loss is calculated using RMS current and MOSFETs Rdson. SR on time is assumed to be 75% of the switching period due to SR sensing delay. Switching loss is neglected as secondary side zero current switching is achieved. The losses on the PCB copper and equivalent series resistor (ESR) of output filter capacitors are estimated based on the previous research. The inputted loss values are shown in Table 2.

C. FEA thermal simulation results

The results of Fig. 8 to Fig. 10 show the temperatures of the transformers (T_x), series inductor (L_r), parallel inductor (L_p), primary side rectifier GaN switches (GaN), and synchronous rectifiers (SR) of the power converter. All three cases are simulated under 25°C ambient temperature. Fig. 8 presents the results for the traditional air-cooled converter. The heat coefficient of moving air convection is assumed to be four times higher than still air. The maximum temperature of the secondary SR MOSFETs is 125°C, which is very close to the device tolerance. The magnetic component temperatures are under 80°C natural convection of the large core surface area.

Fig. 9 shows the results for the conventional single PCB liquid cooling structure. The maximum temperature on the semiconductor switches and PCB is 79°C which is 50% cooler than the passive air-cooling structure. The temperature of magnetic components is higher as the converter was design to prioritize surface mount switch temperature rise. The remaining passive components are much less sensitive compared to the semiconductor devices; therefore, reliability and efficiency are expected improve. These claims will be investigated in experimentation.

Fig. 10 shows the thermal results of the IMLC converter structure with the same losses and ambient temperature. Compared with Fig. 9, the IMLC structure achieves almost the same thermal performance on the GaN FETs, SR MOSFETs and magnetic components. The temperature of active switches is significantly decreased compared with the air-cooling solution. Overall size is reduced by 30% compared to the single-PCB liquid cooled converter.

IV. Verification with Experimental Results

A prototype of the two-layer liquid cooled IMLC power converter is assembled to verify thermal performance. A single-PCB liquid cooled prototype is also assembled to compare to traditional liquid cooling methods. Thermal testing is conducted on the single-layer PCB with air cooling, the single-layer PCB with liquid cooling, and the two-layer IMLC power converter with liquid cooling. The liquid cooling loop consists of a pump, reservoir, radiator with fans, and a cold plate. Distilled water is used as the coolant in all experiments. Each cooling structure is applied to a 1.3kW power converter as discussed in Table 1. All three structures are first tested at 14V output and 70A load current steady-state condition. For the second test operating at 14V output, 95A load current, only the liquid cooled structures are tested to maintain safe operating temperatures.

Fig. 11 shows the results of the air-cooled structure under 70A load. The maximum temperature of the passive components is 59°C on the transformer secondary winding;

Table 2: Power converter loss distribution.

Dissipated heat P_d	GaN FET loss P_{GaN}	Resonant L loss P_{Lr}	Parallel L loss P_{Lp}	Transformer loss P_{Tx}	Secondary SR loss P_{SR}	Secondary PCB loss P_{SP}	Capacitor ESR loss P_C
51.86W	3.49W	3.34W	2.61W	16.38W	19.51W	4.53W	2W

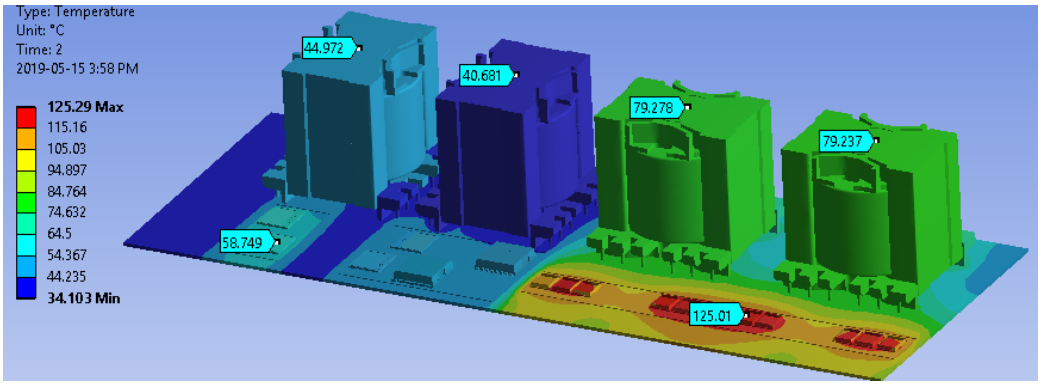

Fig. 8. Thermal simulation of single PCB air cooled layout.

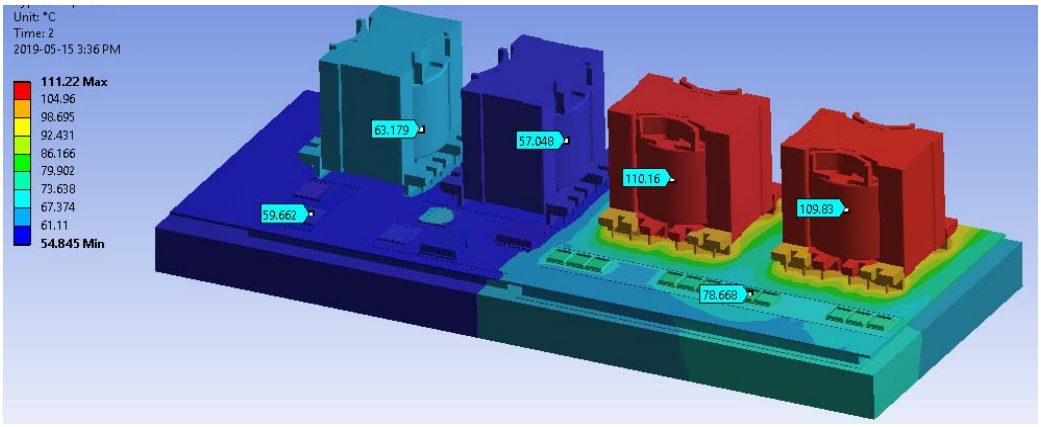

Fig. 9. Thermal simulation of single PCB liquid cooled layout.

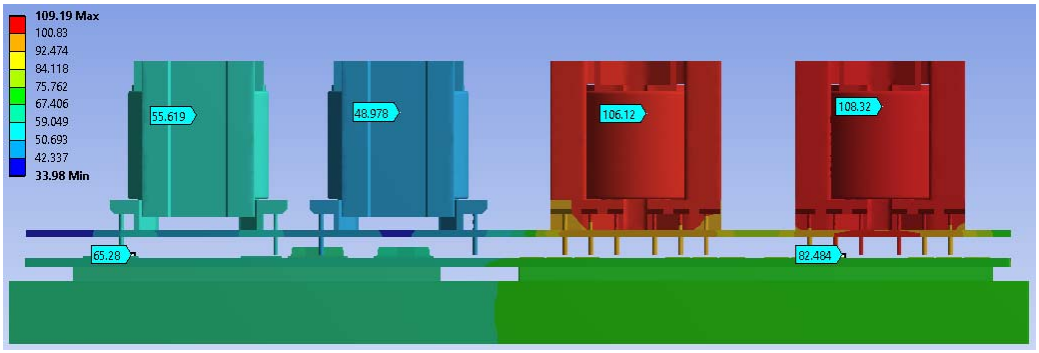

Fig. 10. Thermal simulation of IMLC liquid cooled layout.

and the maximum temperature of semiconductor devices is 84°C on the SR MOSFETs. With a load increase to 95A, the temperature of SR MOSFETs quickly rises to 122°C as shown in Fig. 12. Therefore, the full load condition for the air-cooled structure is well above the attainable heat dissipation of this structure.

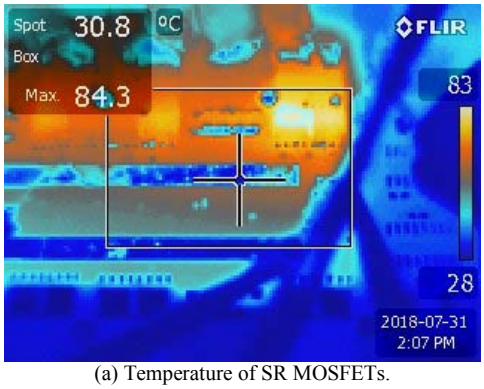

(a) Temperature of SR MOSFETs.

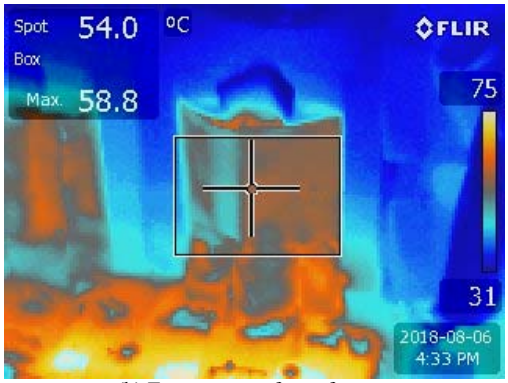

(b) Temperature of transformers

Fig. 11. Temperatures at 70A with air cooling.

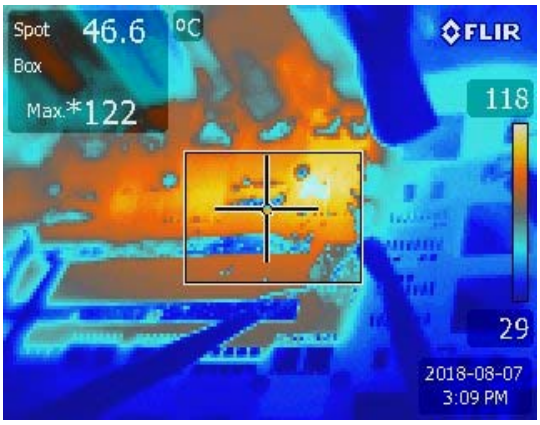

Fig. 12. SR temperature at 95A with air cooling.

Fig. 13 and Fig. 14 demonstrate the improved thermal performance achieved by the single-PCB liquid cooled converter and IMLC converter respectively. The maximum steady state operating temperature of the SR MOSFETs at 95A load current with liquid cooling is 76°C which is more than 46°C lower than air cooled structure. The transformer temperature is 110°C, however these passive devices are less sensitive as they have higher temperature ratings. Thermal images of switches in the IMLC prototype are not applicable due to visual constraints; however, the magnetic component temperatures match the single PCB results very closely. Therefore, SR and GaN temperatures are expected to remain unchanged from the single-PCB liquid cooled structure.

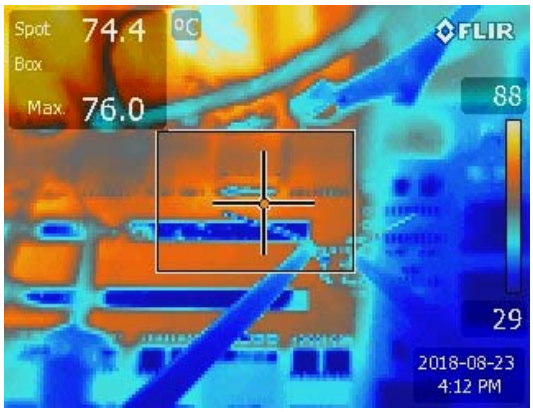

(a) Temperature of SR MOSFETs

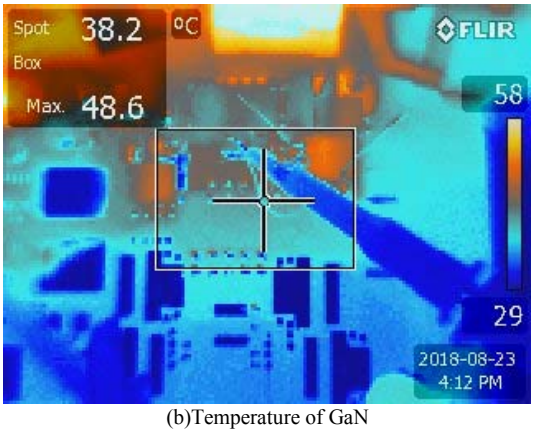

(b)Temperature of GaN

Fig. 13. Temperature at 95A load current with liquid cooling.

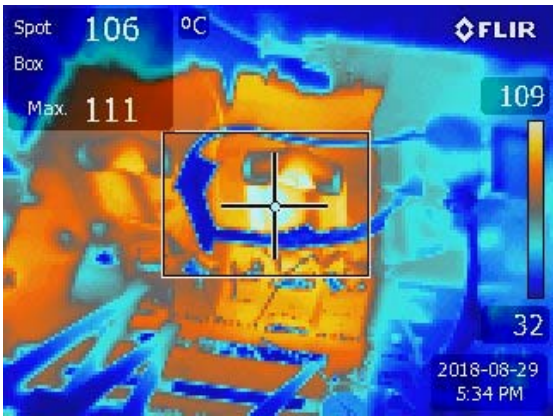

(a) Transformer temperatures

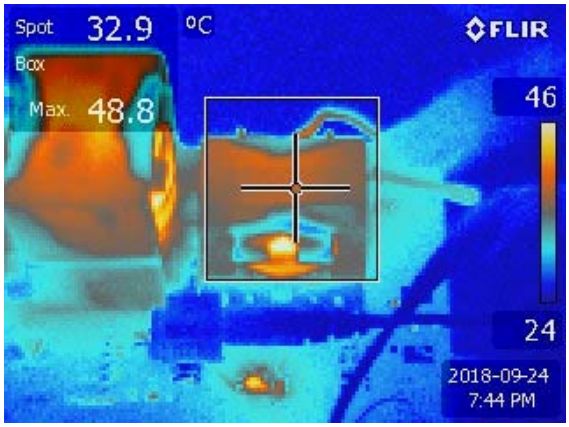

(b) Inductor temperatures

Fig. 14. Temperature at 95A with IMLC structure.

SR MOSFET on-resistance is proportional to temperature. Therefore, for liquid cooled designs, increased heat transfer also reduces on-resistance, decreasing secondary side loss and further reducing SR MOSFET temperature rise. The efficiency curves of air-cooled and liquid-cooled prototypes are shown in Fig. 15. The efficiency at 70A load current condition is improved by 0.6%, while overall efficiency is improved at lighter load conditions. The load condition was not increased above 70A as the air-cooled prototype could not dissipate the required heat at this condition. The experimental results of the air-cooled and liquid-cooled structures show a close agreement with the respective FEA simulations. The liquid cooling solution achieves a 48% temperature rise reduction on active devices, increases the loading capability and improving efficiency by 0.6%. In addition, the 1.3kW power converter with IMLC improves the total package power density by 31% compared to the single PCB layer design.

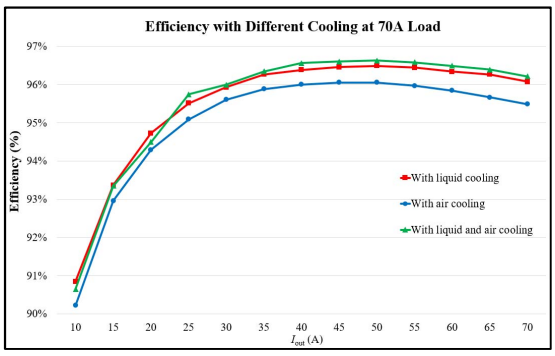

Fig. 15. Efficiency comparison of different thermomechanical designs.

V. Conclusion

This paper proposes a new Integrated Multi-Layer cooling (IMLC) structure for power converters based on multiple PCB layers and integrated liquid cooling. The IMLC structure improves package volume without sacrificing thermal performance based on three design principles: multiple vertically stacked PCB's to utilize three-dimensional space, component sorting by loss to provide heat transfer to high loss components, and integrating bottom mounted cold plate heatsinking for thermal dissipation. FEA thermal modelling is conducted on a 1.3kW power converter for air cooled and liquid cooled structures. Experimental results of air cooling and liquid cooling are compared to verify the heatsinking abilities of the IMLC structure. Integrated liquid-cooling reduces synchronous rectifier temperatures by 46°C in experimental results and improves the efficiency by more than 0.6%. A two-layer IMLC power converter is assembled and achieves 31% greater power density than the single-layer design.

References

[1] F. C. Lee and Q. Li, "High-Frequency Integrated Point-of-Load Converters: Overview," in *IEEE Transactions on Power Electronics*, vol. 28, no. 9, pp. 4127-4136, Sept. 2013.

[2] C. Duan, H. Bai, W. Guo and Z. Nie, "Design of a 2.5-kW 400/12-V High-Efficiency DC/DC Converter Using a Novel Synchronous Rectification Control for Electric Vehicles," in *IEEE Transactions on Transportation Electrification*, vol. 1, no. 1, pp. 106-114, June 2015

[3] Z. Liu, B. Li, F. C. Lee and Q. Li, "High-Efficiency High-Density Critical Mode Rectifier/Inverter for WBG-Device-Based On-Board Charger," in *IEEE Transactions on Industrial Electronics*, vol. 64, no. 11, pp. 9114-9123, Nov. 2017.

[4] L. Wang, W. Liu, D. Malcom and Y. Liu, "An Integrated Power Module Based on the Power-System-In-Inductor Structure," in *IEEE Transactions on Power Electronics*, vol. 33, no. 9, pp. 7904-7915, Sept. 2018.

[5] W. Zhang, F. Wang, D. J. Costinett, L. M. Tolbert and B. J. Blalock, "Investigation of Gallium Nitride Devices in High-Frequency LLC Resonant Converters," in *IEEE Transactions on Power Electronics*, vol. 32, no. 1, pp. 571-583, Jan. 2017

[6] J. L. Lu, D. Chen and L. Yushyna, "A high power-density and high efficiency insulated metal substrate based GaN HEMT power module," 2017 *IEEE Energy Conversion Congress and Exposition (ECCE)*, Cincinnati, OH, 2017, pp. 3654-3658.

[7] J. L. Lu, R. Hou and D. Chen, "Opportunities and design considerations of GaN HEMTs in ZVS applications," 2018 *IEEE Applied Power Electronics Conference and Exposition (APEC)*, San Antonio, TX, 2018, pp. 880-885

[8] L. Boteler, "Thermal Design of Power Electronics," *2019 IEEE Applied Power Electronics Conference and Exposition (APEC)*, Anaheim, CA, 2019, Educational Tutorial.

[9] Z. Liang, P. Ning, F. Wang and L. Marlino, "A Phase-Leg Power Module Packaged with Optimized Planar Interconnections and Integrated Double-Sided Cooling," in *IEEE Journal of Emerging and Selected Topics in Power Electronics*, vol. 2, no. 3, pp. 443-450, Sept. 2014.

[10] Numakura, K., Emori, K., Yoshino, Y., Hayami, Y., Hayashi, T., (2016, September). Direct-cooled power module with a thick Cu heat spreader featuring a stress-suppressed structure for EV/HEV inverters. In 2016 *IEEE Energy Conversion Congress and Exposition (ECCE)*. IEEE.

[11] R. Hou and A. Emadi, "Applied Integrated Active Filter Auxiliary Power Module for Electrified Vehicles with Single-Phase Onboard Chargers," in *IEEE Transactions on Power Electronics*, vol. 32, no. 3, pp. 1860-1871, March 2017

[12] R. Hou and A. Emadi, "A Primary Full-Integrated Active Filter Auxiliary Power Module in Electrified Vehicles with Single-Phase Onboard Chargers," in *IEEE Transactions on Power Electronics*, vol. 32, no. 11, pp. 8393-8405, Nov. 2017

[13] M. Vuckovic and N. Depret, "Impacts of local cooling technologies on air cooled data center server performance: Test data analysis of Heatsink, Direct Liquid Cooling and passive 2-Phase Enhanced Air Cooling based on Loop Heat Pipe," 2016 32nd *Thermal Measurement, Modeling & Management Symposium (SEMI-THERM)*, San Jose, CA, 2016, pp. 71-80.

[14] F. Liu, B. Duan, X. Yu, R. Wu and X. Luo, "A study on a simplified liquid cooling system with a pump serving as cold plate," in *International Conference on Electronic Packaging Technology (ICEPT)*, Harbin, China, 2017.

[15] B. Akselband, K. Whitenack and D. Goldman, "Copper Cold Plate Technology Comparison," in *Thermal and Thermomechanical Proceedings 10th Intersociety Conference on Phenomena in Electronics Systems*, San Diego, CA, 2006.

[16] K. Hwang, S. W. Lee, S. W. Karng and S. Y. Kim, "Thermal performance of non-metallic two-phase cold plates for humanoid robot cooling," in *Intersociety Conference on Thermal and Thermomechanical Phenomena in Electronic Systems*, Orlando, FL, 2008.

[17] M. Parlak and V. Yagci, "Thermal Expansion Investigation of Liquid Cold Plate with Varying Ambient Temperature at Storage," in *IEEE Intersociety Conference on Thermal and Thermomechanical Phenomena in Electronic Systems (ITherm)*, San Diego, CA, 2018.

[18] G. R. Wagner, J. R. Schaadt, J. Dixon, G. Chan, W. Maltz, K. Mostafavi and D. Copeland, "Test results from the comparison of three liquid cooling methods for high-power processors," in *IEEE ITHERM Conference*, Las Vegas, 2016.

[19] Z. Hu, Y. Qiu, L. Wang and Y. Liu, "An Interleaved LLC Resonant Converter Operating at Constant Switching Frequency," *in IEEE Transactions on Power Electronics*, vol. 29, no. 6, pp. 2931-2943, June 2014.

[20] Y. Kim, C. Oh, W. Sung and B. K. Lee, "Topology and Control Scheme of OBC–LDC Integrated Power Unit for Electric Vehicles," in *IEEE Transactions on Power Electronics*, vol. 32, no. 3, pp. 1731-1743, March 2017

[21] Z. Liu, R. Yu, T. Chen, Q. Huang and A. Q. Huang, "Real-time adaptive timing control of synchronous rectifiers in high frequency GaN LLC converter," *2018 IEEE Applied Power Electronics Conference and Exposition (APEC)*, San Antonio, TX, 2018, pp. 2214-2220.

[22] G. Zulauf, S. Park, W. Liang, K. N. Surakitbovorn and J. Rivas-Davila, "COSS Losses in 600 V GaN Power Semiconductors in Soft-Switched, High- and Very-High-Frequency Power Converters," in *IEEE Transactions on Power Electronics*, vol. 33, no. 12, pp. 10748-10763, Dec. 2018.

[23] C. R. Sullivan and R. Y. Zhang, "Simplified design method for litz wire," *2014 IEEE Applied Power Electronics Conference and Exposition - APEC 2014*, Fort Worth, TX, 2014, pp. 2667-2674.

[24] W. Liu, L. Wang, S. Webb, Y. F. Liu and D. Malcolm, "A Modified Equivalent Circuit Based Electro-Thermal Model for Integrated POL Power Modules," in *IEEE Energy Conversion Congress & Expo (ECCE) 2017*, Cincinati,Ohio, USA, Oct 2017, pp. 1366-1373

[25] Hu Wenshan, Yi Lingsong, Liu Zhiwei and Yan Hui, "Loss analysis and improvement of all parts of magnetic resonant wireless power transfer system," 2015 Chinese Automation Congress (CAC), Wuhan, 2015, pp. 2251-2256.